https://doi.org/10.5194/egusphere-2025-1375
Preprint. Discussion started: 2 April 2025

Modeling impacts of ozone on gross primary production across European forest ecosystems using JULES

Inês Vieira[1*], Félicien Meunier[1,2], Maria Carolina Duran Rojas[3], Stephen Sitch[3], Flossie Brown[4], Giacomo Gerosa[5], Silvano Fares[6], Pascal Boeckx[2], Marijn Bauters[1] and Hans Verbeeck[1]

[1] Q-ForestLab, Laboratory of Quantitative Forest Ecosystem Science, Department of Environment, Ghent University, Gent, Belgium

[2] ISOFYS, Isotope Bioscience Laboratory, Department of Green Chemistry and Technology, Ghent University, Gent, Belgium

[3] Faculty of Environment, Science & Economy, University of Exeter, Exeter, United Kingdom

[4] Institute for Atmospheric and Climate Science, ETH Zurich, Zurich, Switzerland

[5] Faculty of Mathematical, Physical and Natural Sciences, Università Cattolica del Sacro Cuore, Brescia, Italy

[6] Institute for Agriculture and Forestry Systems in the Mediterranean, National Research Council of Italy, Naples, Italy

Correspondence to: Inês Vieira (ines.dossantosvieira@ugent.be)

Abstract. This study investigates the effects of tropospheric ozone (O_3), a potent greenhouse gas and air pollutant, on European forests, an issue lacking comprehensive analysis at the site level. Unlike other greenhouse gases, O_3 in the troposphere is primarily formed through photochemical reactions, significantly impairing vegetation productivity and carbon fixation, thereby impacting forest health and ecosystem services. We utilise data from multiple European flux tower sites and integrate statistical and mechanistic modelling approaches to simulate O_3 impacts on photosynthesis and stomatal conductance. The study examines six key forest sites across Europe: Hyytiälä and Värriö (Finland), Brasschaat (Belgium), Fontainebleau-Barbeau (France), Bosco-Fontana, and Castelporziano 2 (Italy), representing boreal, temperate, and Mediterranean climates. These sites provide a diverse range of environmental conditions and forest types, enabling a comprehensive assessment of O_3 effects on Gross Primary Production (GPP). We calibrated the Joint UK Land Environment Simulator (JULES) model using observed GPP data to simulate different O_3 exposure sensitivities. Incorporating O_3 effects improved the model's accuracy across all sites, although the magnitude of improvement varied depending on site-specific factors such as vegetation type, climate, and ozone exposure levels. The GPP reduction due to ozone exposure varied considerably across sites, with annual mean reductions ranging from 1.04% at Värriö to 6.2% at Bosco-Fontana. These findings emphasise the need to account for local environmental conditions when assessing ozone stress on forests. This study highlights the strengths and limitations of the JULES model in representing O_3-vegetation interactions, providing critical insights for predicting forest health and productivity under future air pollution scenarios. The model effectively captures the diurnal and seasonal variability of GPP

and its sensitivity to O_3 stress, particularly in boreal and temperate forests. However, its performance is limited in Mediterranean ecosystems, where pronounced O_3 peaks and environmental stressors such as high vapor pressure deficit exacerbate GPP declines, pointing to the need for improved parameterisation and representation of site-specific processes. By integrating in situ measurements, this research contributes to developing targeted strategies for mitigating the adverse effects of O_3 on forest ecosystems.

1 Introduction

Ground-level ozone (O_3) is a greenhouse gas and an air pollutant with a strong oxidative capacity being responsible for negatively impacting human health (Nuvolone et al., 2018; Lu and Yao, 2023), water and carbon cycles (Sitch et al., 2007; Lombardozzi et al., 2015), agriculture and crop production (Van Dingenen et al., 2009; Feng et al., 2022; Li et al., 2022) and vegetation productivity (Ainsworth et al., 2012; Yue and Unger, 2014; Ainsworth et al., 2019; Savi et al., 2020). In the troposphere O_3 is not emitted directly, contrary to other greenhouse gases, such as carbon dioxide (CO_2) and methane (CH_4). The majority of O_3 (about 90%) is generated by the photochemical oxidation of its precursor gases (natural and anthropogenic), such as CH_4, carbon monoxide (CO), and volatile carbon compounds (VOCs) in the presence of nitrogen oxides (NOx). The remaining 10% is from the influx of ozone from the stratosphere. On the other hand, tropospheric O_3 is primarily removed through chemical destruction and dry deposition to terrestrial surfaces that occurs via stomatal (Fowler et al., 2009; Ducker et al., 2018; Clifton et al., 2020) and non-stomatal pathways (Zhang et al., 2003; Wong et al., 2022).

Stomatal O_3 uptake damages vegetation by causing cell death and decreasing carbon fixation (Li et al., 2019), which in turn leads to reduced productivity (Ainsworth et al., 2012) and early senescence (Gielen et al., 2007). In particular, it reduces gross primary production (GPP), the gross carbon uptake via photosynthesis, a measure of ecosystem productivity (Proietti et al., 2016; Cailleret et al., 2018; Grulke et al., 2019). Therefore, incorporating a representation of ozone damage to plants in land surface and Earth System models (LSMs and ESMs) is essential because many regions experience potentially damaging O_3 concentrations. However, while most studies agree that O_3 exposure results in significant reductions in GPP, the reduction varies with measurement location or assumptions used in the models. For example, Sitch et al. (2007) predicted a decline in global GPP of 14 to 23% by 2100. Lombardozzi et al. (2015) predicted a 10.8% decrease in present-day (2002–2009) GPP globally. Also, Yue and Unger (2014) found that O_3 damage decreases GPP by 4 %–8 % on average in the eastern US, leading to significant 11 %–17 % decreases on the east coast.

In Europe, surface O_3 pollution poses a significant air quality challenge, particularly in southern Europe, where high solar radiation intensifies O_3 formation due to interactions between traffic emissions and industrial activities (Sicard et al., 2021). Currently, the European standard used to protect vegetation against negative impacts of O_3 is the Accumulated Ozone over a Threshold of 40 ppb (AOT40), i.e. the cumulative exposure to hourly O_3 concentrations above 40 ppb over the daylight hours of the growing season (Anav et al., 2017; Proietti et al., 2021). However, the O_3 uptake through stomata is a better metric for assessing plant damage because it estimates the actual quantity of O_3 entering the leaf tissues (Anav et al., 2016; Sicard et al.,

https://doi.org/10.5194/egusphere-2025-1375
Preprint. Discussion started: 2 April 2025

2016). High ambient O_3 levels may not damage plants when drought and/or other environmental stressors limit the stomatal aperture (Shang et al., 2024). Therefore, flux-based approaches were developed to assess the effects of O_3 on vegetation. This method quantifies leaf O_3 uptake and the dose that actually enters the plant tissue via stomata and considers the environmental constraints that may limit optimal stomatal conductance. For example, Proietti et al. (2016) performed a comprehensive study on 37 European forest sites during the period of 2000-2010 to assess surface O_3 effects on GPP. In this study, the DO_3SE (Deposition of O_3 and Stomatal Exchange) model (Emberson et al., 2001) was used to estimate ozone uptake/stomatal ozone flux using the Jarvis multiplicative method for stomatal conductance (Jarvis, 1976). The results showed that GPP was reduced between 0.4% and 30% annually across different sites. Also, Anav et al. (2011) showed, using a land surface model coupled with a chemistry transport model, a 22% reduction in yearly GPP and a 15-20% reduction in leaf area index (LAI) due to O_3 exposure, with the most substantial impacts occurring during the summer months.

Interestingly, not all studies have found significant negative effects of O_3 on GPP. For instance, research on a Scots pine stand in Belgium over 15 years found no significant O_3 effects on GPP despite high stomatal O_3 uptake (Verryckt et al., 2017). This suggests that the impact of O_3 may vary depending on specific forest types and local conditions. Satellite observations have also been utilised to assess O_3-induced GPP reductions, estimating a decrease of 0.4-9.6% across European forests from 2003-2015. These findings align with previous estimates and highlight soil moisture as a critical interacting variable influencing GPP reductions, particularly in Mediterranean regions (Vargas et al., 2013). Therefore, while the negative effects of O_3 on GPP in European forests are well-documented, the extent of these impacts can vary significantly based on regional conditions, forest types, methodological approaches, and it is not clear what drives the local differences. Understanding these variations is crucial for accurately assessing the broader implications of O_3 on forest productivity and ecosystem services. This gap in the literature underscores the need for detailed studies that evaluate the influence of ozone on forest productivity in Europe using advanced process-based models. This study provides a detailed, site-level analysis of O_3 impacts on GPP across European forests, leveraging local *in situ* measurements of O_3, CO_2 exchange, and meteorological data to optimise the Joint UK Land Environment Simulator (JULES) model. Our objectives are to quantify O_3-induced GPP limitations and assess model improvements through the incorporation of ozone damage mechanisms. Specifically, we aim to address the following research questions:

1. To what extent can we improve GPP simulations for European forests of a process-based model by incorporating plant sensitivity to ozone?
2. To what extent does ozone limit GPP across European forests?
3. How do ozone impacts interact with other environmental factors, and how can an optimised model help us understand these mechanisms, particularly on high-ozone days?

To achieve these objectives, we combined a multi-year eddy covariance flux tower dataset across a latitudinal gradient in Europe across six sites in boreal, temperate, and Mediterranean forests and statistical and process-based models, providing a comprehensive understanding of ozone's effects on GPP.

https://doi.org/10.5194/egusphere-2025-1375
Preprint. Discussion started: 2 April 2025

2 Materials and Methods

2.1 Study Area

We investigated six sites along a European latitudinal gradient in four countries: Finland, Belgium, France and Italy (Fig. 1, Table 1), belonging to the Integrated Carbon Observation System (ICOS, https://www.icos-cp.eu/ , last access: 20 September 2024). These sites span boreal, temperate, and Mediterranean climates, representing diverse forest ecosystems with varying ozone exposure, productivity, and environmental conditions.

The Värriö site (FI-Var) of the University of Helsinki is located in Värriö strict nature reserve, Salla, Finnish Lapland. The area lies 130 km north of the Arctic Circle and 6 km from the Finnish Russian border. The flux tower is located at the arctic-alpine timberline on the top plateau of the hill of Kotovaara, at 395 m a.s.l, and surrounded by a homogeneous and relatively open 10m tall Scots Pine (*Pinus sylvestris* L.) forest. The leaf area index (LAI) varies between 0.0013 and 0.68 m^2m^{-2} (Dengel et al., 2013). The Hyytiälä forest (FI-Hyy) boreal site is located 220 km NW from Helsinki, Finland. The station is dominated by Scots pine (*Pinus sylvestris* L.), Norway spruce, and birch on a slightly hilly terrain. The LAI varies between 0.45 and 3.04 m^2m^{-2} (Schraik et al., 2023). The Brasschaat site (BE-Bra) is a forest located 20 km northeast of Antwerp, Belgium. The study site consists of a 150-ha mixed coniferous/deciduous forest dominated by Scots pine. The LAI varies between 1 and 1.5 m^2m^{-2} (Op de Beeck et al., 2010). Fontainebleau–Barbeau forest (FR-Fon) is located 53 km southeast of Paris, France. Fontainebleau–Barbeau is a deciduous forest mainly composed of mature sessile oak (*Quercus petraea* (Matt.) Liebl). The average LAI over the 2012–2018 period was 5.8 m^2m^{-2}, ranging from 4.6 to 6.8 m^2m^{-2} (Soudani et al., 2021). The Bosco-Fontana site (IT-BFt) is a 233-ha forest composed mainly of mature Oak-Hornbeam (*Carpinus betulus*) at Po Valley, a few kilometres from Mantova, Italy. The LAI ranges between 0.9 and 3.0 m^2m^{-2} (Gerosa et al., 2022). The Castelporziano 2 site (IT-Cp2) is located in the Presidential Estate of Castelporziano, around 25 km southwest of the centre of Rome, Italy. Castelporziano covers an area of about 6000 ha of undisturbed Mediterranean maquis, oak and pine forests. The experimental site is located inside a pure Holm Oak (*Quercus ilex*) stand with some shrubs in the understory. The LAI varies between 0.5 and 4.5 m^2m^{-2} (Gratani and Crescente, 2000). More details about each site are available in Table 1.

Table 1: Overview of the study sites.

Site	Värriö	Hyytiälä	Brasschaat	Fontainebleau-Barbeau	Bosco-Fontana	Castelporziano 2
Acronym	**FI-Var**	**FI-Hyy**	**BE-Bra**	**FR-Fon**	**IT-BFt**	**IT-Cp2**
Country	Finland	Finland	Belgium	France	Italy	Italy
Latitude (°)	67.75	61.85	51.30	48.47	45.19	41.70

https://doi.org/10.5194/egusphere-2025-1375
Preprint. Discussion started: 2 April 2025

Longitude (°)	29.61	24.29	4.52	2.78	10.74	12.36
Elevation (m a.s.l.)	395	181	16	103	23	19
Forest type	Evergreen Needleleaf Forests	Evergreen Needleleaf Forests	Mixed Forests	Deciduous Broadleaf Forests	Deciduous Broadleaf Forests	Evergreen Broadleaf Forest
Meteorological dataset	2017-2023	1996-present	1996-present	2005-present	2013-2020	2012-present
O_3 concentration	2017-2023	1996-present	1996-2020	2014-2020	2013-2020	2013-2014
Fluxes (GPP, LE)	2017-2023	1996-present	1999-present	2005-present	2012-present	2012-present
Mean annual temperature (°C)	-0.5	3.5	10.5	11.4	14.5	16.43
Mean annual precipitation (mm)	601.0	711.0	920.7	678.9	697.0	601.0
Mean annual O_3 concentration (ppb)	31.85	28.37	23.78	30.08	34.47	27.72
Maximum O_3 concentration (ppb)	109.57	89.32	143.0	139.25	144.71	119.84
Mean summer AOT40 (ppb.hours)	336.96	1538.42	5406.77	41912.28	20084.90	13172.03

https://doi.org/10.5194/egusphere-2025-1375
Preprint. Discussion started: 2 April 2025

Mean summer O_3 (ppb)	28.37	32.17	31.67	71.71	42.30	45.98
Mean annual GPP (tC ha^{-1} yr^{-1})	470.1	470.1	1181	1452.9	2069.3	1683.6
Peak LAI (m^2m^{-2})	0.68 (Dengel et al., 2013)	3.04 (Schraik et al., 2023)	1.31 (Op de Beeck et al., 2010)	6.8 (Soudani et al., 2021)	3.0 (Gerosa et al., 2022)	4.76 (Fares et al., 2013)

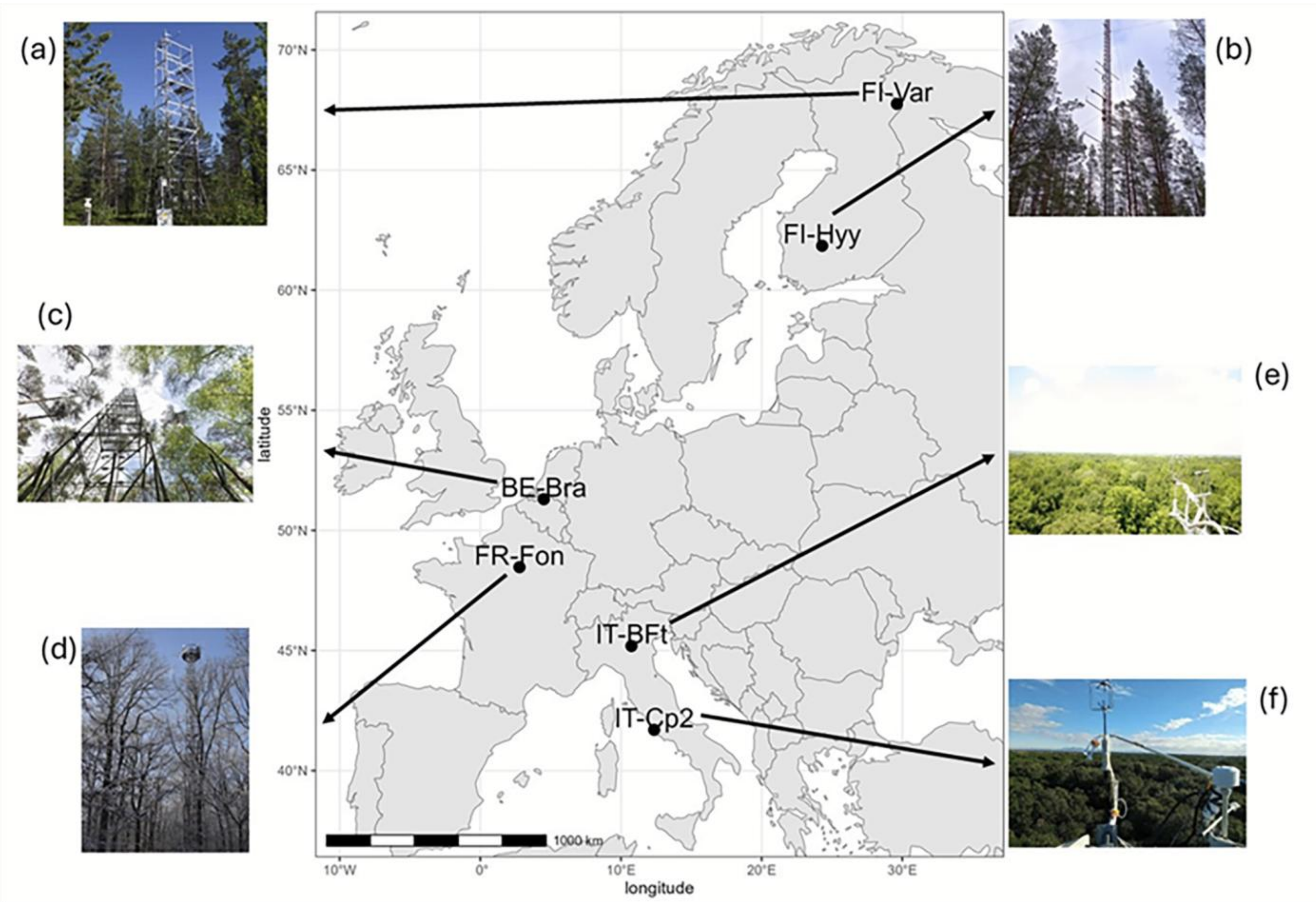

Figure 1: Geographical location of the six study sites across Europe: (a) Värriö, Finland (FI-Var),(b) Hyytiälä, Finland (FI-Hyy), (c) Brasschaat, Belgium (BE-Bra), (d) Fontainebleau-Barbeau, France (FR-Fon), (e) Bosco-Fontana, Italy (IT-BFt) and (f) Castelporziano 2, Italy (IT-Cp2). All photos were retrieved from the ICOS website (https://www.icos-cp.eu/, last access: 20 September 2024)

https://doi.org/10.5194/egusphere-2025-1375
Preprint. Discussion started: 2 April 2025

2.2 Meteorological, Ozone, and Ecosystem Flux Datasets

For each site, the following meteorological variables were available on the ICOS data portal: air temperature (TA, °C), relative humidity (RH, %), short-wave radiation (SW, Wm^{-2}), precipitation (P, mm), atmospheric pressure (PA, kPa) and vapour pressure deficit (VPD, hPa). Measured half-hourly O_3 concentration data (ppb, Fig. 2) were provided by site principal investigators. The half-hourly Gross Primary Production data (GPP, $\mu mol\ m^{-2}s^{-1}$) and Latent Heat (LE, $W\ m^{-2}$) were estimated for the ecosystem from net-carbon flux measurements acquired by an eddy covariance system in each site (Warm Winter 2020 Team, ICOS Ecosystem Thematic Centre, 2022). All meteorological data, GPP and LE, are freely available on the ICOS portal. The data are in the standard format used for the ICOS L2 ecosystem. The processing has been done using the ONEFlux processing pipeline (https://github.com/icos-etc/ONEFlux) and is fully compliant and integrable with the FLUXNET2015 release (https://fluxnet.fluxdata.org/). Basic site-level statistics and the data extent are reported in Table 1.

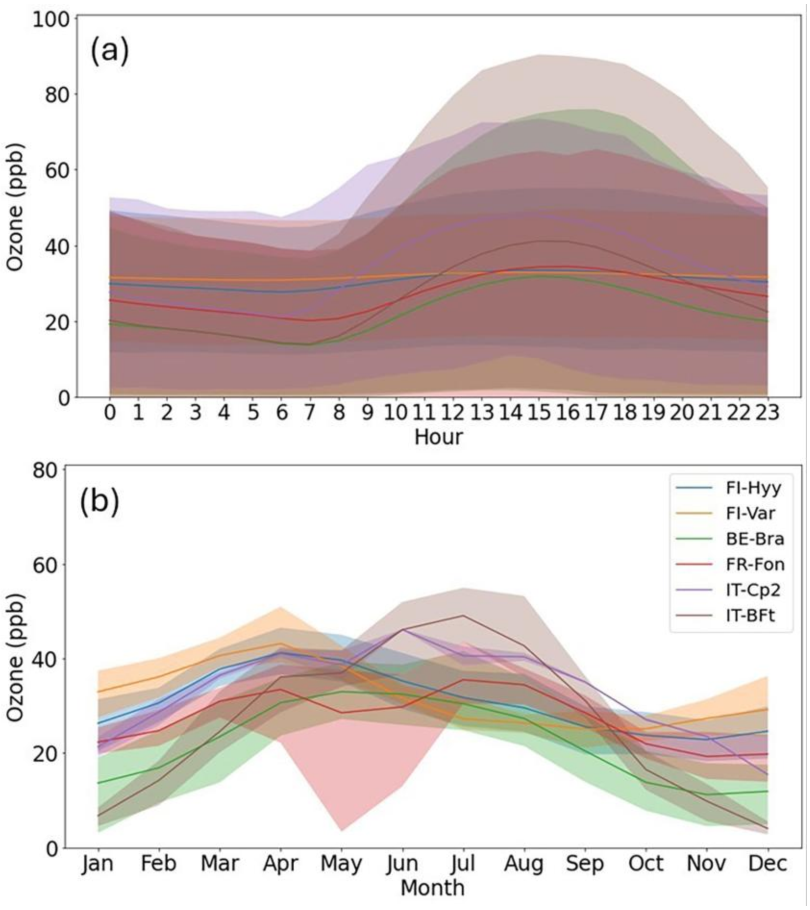

Figure 2: Diurnal (a) and seasonal (b) cycles of ozone concentrations at each site. Shaded areas indicate 95% confidence intervals. Site acronyms are defined in Table 1.

https://doi.org/10.5194/egusphere-2025-1375
Preprint. Discussion started: 2 April 2025

2.3 Statistical analysis: partial correlations

To investigate the specific impact of O_3 on GPP, we used a partial correlation analysis, which measures the strength of a relationship between two variables while controlling for the effect of one or more other variables. This analysis isolates the effects of O_3 on GPP, independent of key environmental drivers such as air temperature, short-wave radiation, and vapour pressure deficit (VPD). Despite this control, subsetting the dataset remains valuable for examining the residual impacts of O_3 under specific environmental conditions. These subsets—summer months and midday hours—represent periods of peak biological activity and photochemical reactions, and, therefore, potential O_3 damage. For example, during the summer, ozone concentrations and GPP are generally higher, while during midday, radiation and photosynthesis peak, likely increasing O_3 uptake through stomata. Subsetting, therefore, helps reveal context-specific dynamics and whether the impacts of O_3 are amplified under these conditions. We used the Python package *Pingouin* (Vallat, 2018) to perform the partial correlations and compute the correlation coefficients and their corresponding significance levels (p-values). To assess the relationship between GPP and O_3, partial correlations were computed under four configurations for each site:

1) Using the entire dataset across all seasons.
2) Use summer months only (June, July, and August) when O_3 levels are elevated and foliage is fully developed.
3) Restricting the analysis to the period between 12:00 and 16:00, coinciding with peak radiation, photosynthesis, and O_3 levels.
4) Combining conditions (2) and (3), focusing on summer midday data.

2.4 JULES land surface model

This study utilises JULES version 7.4, a community land surface model widely applied as both a standalone model and the land surface component of the Met Office Unified Model (https://jules.jchmr.org/, last access: 14 July 2024). We employed the offline version of JULES, where we incorporated *in situ* observed meteorological, CO_2 and O_3 datasets. Detailed descriptions of JULES can be found in Best et al. (2011), Clark et al. (2011), and Harper et al. (2016). The Farquhar photosynthesis scheme (Farquhar et al., 1980), as implemented by Oliver et al. (2022), models the leaf-level biochemistry of photosynthesis (A, kg C m^{-2} s^{-1}) for C_3 vegetation, while the Medlyn scheme (Medlyn et al., 2011) is used to calculate stomatal conductance (g_p, m s^{-1}). The Medlyn approach optimises the stomatal aperture to balance carbon gain with water loss. The stomatal conductance (g_p, m s^{-1}) is represented as:

$$g_p = 1.6 R T_l \frac{A}{c_a - c_i} \tag{1}$$

where the factor 1.6 represents the conductance for water vapour, R is the universal gas constant (J mol^{-1} K^{-1}), T_l is the leaf surface temperature (K), and c_a and c_i (both Pa) are the leaf surface and internal CO_2 partial pressures, respectively. In this scheme, c_i is calculated as:

https://doi.org/10.5194/egusphere-2025-1375
Preprint. Discussion started: 2 April 2025

$$c_i = c_a \times \frac{g_1}{g_1 + \sqrt{d_q}} \quad (2)$$

where d_q is the specific humidity deficit at the leaf surface (kPa), and g_1 ($kPa^{0.5}$) represents the sensitivity of g_p to the assimilation rate, which is Plant Functional type (PFT) dependent. Photosynthesis and stomatal conductance are modelled to respond to changes in environmental drivers (temperature, VPD, incoming radiation, CO_2 concentration and water availability). The impact of soil moisture availability on stomatal conductance is modelled using a dimensionless soil water stress factor (β, unitless) related to the actual soil water content in each layer (θ_k, $m^3\,m^{-3}$) and the critical water content (θ_{crit}, $m^3\,m^{-3}$) and water contents at the wilting point (θ_{wilt}, $m^3\,m^{-3}$) and at which the plant starts to become water stressed (θ_{upp}, $m^3\,m^{-3}$) (Harper et al., 2021):

$$\beta = \begin{cases} 1 & \text{if } \theta_k \geq \theta_{\text{upp}} \\ \frac{\theta_k - \theta_{\text{wilt}}}{\theta_{\text{upp}} - \theta_{\text{wilt}}} & \text{if } \theta_{\text{wilt}} \leq \theta_k < \theta_{\text{upp}} \\ 0 & \text{if } \theta_k < \theta_{\text{wilt}} \end{cases}$$

θ_{upp} is a function of θ_{crit}, and p_0 (unitless), a PFT-dependent parameter, a threshold at which the plant starts to experience water stress:

$$\theta_{upp} = \theta_{wilt} + (\theta_{crit} - \theta_{wilt})(1 - p_0) \quad (4)$$

2.4.1 JULES: Ozone damage scheme

The ozone damage scheme implemented in JULES follows the approach of Sitch et al. (2007), incorporating a damage factor (F) to quantify O_3-induced reductions in photosynthesis and stomatal conductance. The modified equations for photosynthesis (A_{net}) and stomatal conductance (g_s) under O_3 stress are:

$$A_{net} = A \times F \quad (5)$$

$$g_s = g_p \times F \quad (6)$$

where A and g_p are the photosynthesis and the stomatal conductance without O_3 effects, respectively. The damage factor is given by:

https://doi.org/10.5194/egusphere-2025-1375
Preprint. Discussion started: 2 April 2025

$$F = 1 - a \times max[F_{O3} - FO3_{crit}, 0] \quad (7)$$

where F_{O3} is the O_3 deposition flux through stomata (mmol m^{-2} s^{-1}), F_{O3crit} is the threshold for stomatal O_3 uptake (nmol m^{-2} s^{-1}), and 'a' is the gradient of the O_3 dose-response function (nmol^{-1} m^2 s). Both 'a' and $FO3_{crit}$ are plant functional type (PFT) specific parameters. The parameter 'a' determines the slope of the ozone dose-response function and represents how sensitive photosynthesis and stomatal conductance are to O_3 uptake. In JULES, 'a' has two default values for each PFT, corresponding to "high" and "low" sensitivities to ozone. These two values allow for the exploration of variability in plant responses to ozone stress, providing a range of potential outcomes. The flux of O_3 to the stomata (F_{O3}) is modelled using a flux gradient approach:

$$F_{O3} = \frac{[O_3]}{r_a + \frac{k_{O3}}{g_s}} \quad (8)$$

where $[O_3]$ is the molar concentration of O_3 above the canopy (nmol m^{-3}), r_a is the aerodynamic and boundary layer resistance (s m^{-1}) and k_{O3} = 1.67 (dimensionless) accounts for the relative difference in diffusivities of O_3 and H_2O through leaf stomata.

2.4.2 Calibration of JULES with and without ozone

In this study, we applied an optimisation approach to calibrate the photosynthesis and stomatal conductance modules in JULES for each site using flux tower datasets. This calibration was performed at a half-hourly resolution, ensuring the optimisation captures short-term variability in GPP responses to environmental drivers. We focused on the summer months (June to August) when O_3 concentrations are typically higher (Table 1, Figure 2), leaves are fully developed, and phenological effects that strongly influence seasonal GPP trends are minimised.

Optimisation approach

We employed a two-step calibration approach, conducting separate simulations with and without O_3 effects. We employed the L-BFGS-B algorithm, a computationally efficient optimisation method. Unlike the standard BFGS algorithm, which uses dense Hessian approximations and is memory-intensive, L-BFGS-B employs a limited-memory approach, reducing computational complexity by approximating the Hessian matrix with a subset of vectors. This efficiency makes L-BFGS-B particularly suitable for optimising a large number of parameters, as required in this study. The objective function for L-BFGS-B was the Root Mean Square Error (RMSE) between the observed and modelled GPP values. By minimising RMSE, we aimed to reduce discrepancies between model predictions and observations, thereby improving the model's predictive accuracy.

Step 1: Optimisation without O_3 effects

For the simulations without O_3, we optimised a total of five physiological parameters related to stomatal conductance, photosynthesis, and plant water stress response (Table 2):

1. g_1: a parameter related to the stomatal conductance model, which determines the sensitivity of stomatal conductance to the assimilation rate.
2. Three photosynthetic parameters:

https://doi.org/10.5194/egusphere-2025-1375
Preprint. Discussion started: 2 April 2025

- J_{max}:V_{cmax}: the ratio of the maximum potential electron transport rate at 25°C (J_{max}) to Rubisco's maximum rate of carboxylation at 25°C (V_{cmax}).
- i_v and s_v: the intercept and slope of the linear relationship between Vc_{max} and N_a, the leaf nitrogen per unit area: $V_{cmax} = i_v + s_v N_a$ (7)

  where N_a is calculated as the product of the Leaf mass per unit area and the top-leaf nitrogen concentration.

3. p_0: a parameter describing the plant transpiration response to soil moisture, representing the threshold at which the plant begins to experience drought stress.

Step 2: Optimisation with O_3 effects

For simulations with O_3, we extended the optimisation to include two additional ozone-specific parameters:

1. $FO3_{crit}$: the critical flux of O_3 to vegetation, , representing the threshold above which O_3 begins to damage photosynthesis and stomatal conductance.
2. a: an empirical PFT-specific O_3 sensitivity parameter that determines the slope of the O_3 dose-response function.

The optimisation process for simulations with O_3 involved two steps:

1. **Initial optimisation**: The same five physiological parameters as in the no-O_3 simulations were optimised, along with F and a.
2. **Local refinement**: To further improve model accuracy under O_3 stress conditions, we performed a local refinement of $FO3_{crit}$ and a. Using the optimised parameter set from the initial step, we systematically explored a fine grid of values around the best-performing $FO3_{crit}$ and a. Step sizes ranging from 0.005 to 0.025 were used to refine the parameter estimates. Model performance was evaluated for each simulation using RMSE, and the best parameter set was selected based on its agreement with observed half-hourly GPP values.

Model configurations

In total, we considered two types of simulations (Figure 3):

1. Default simulations: Site-level runs using default model parameters (Oliver et al., 2022; Harper et al., 2016; Harper et al., 2021), with and without O_3 effects.
2. Optimised simulations: Site-level runs using optimised parameters, with and without O_3 effects.

For optimised simulations without O_3, the calibrated parameters included g_1, J_{max}:V_{cmax}, i_v, s_v, and p_0. For optimised simulations with O_3, we additionally calibrated $FO3_{crit}$ and a.

https://doi.org/10.5194/egusphere-2025-1375
Preprint. Discussion started: 2 April 2025

Table 2: Default parameter values of the JULES for each site.

Parameter	Name	Unit	FI-Hyy	FI-Var	BE-Bra	FR-Fon	IT-BFt	IT-Cp2
g_1	Sensitivity of the stomatal conductance to the assimilation rate	$kPa^{0.5}$	2.35	2.35	2.35	4.45	4.45	3.37
$J_{max}:V_{cmax}$	Ratio of J_{max} to V_{cmax} at 25 deg C	-	1.48	1.48	1.48	1.78	1.78	1.63
i_v	Intercept of the linear relationship between V_{cmax} and N_a	μmol CO_2 m^{-2} s^{-1}	6.32	6.32	6.32	5.73	5.73	3.90
s_v	Slope of the linear relationship between V_{cmax} and N_a	μmol CO_2 gN^{-1} s^{-1}	18.15	18.15	18.15	29.81	29.81	28.40
p_0	threshold at which the plant starts to experience water stress	-	0	0	0	0	0	0
$FO3_{crit}$	Critical flux of O_3 to vegetation	nmol m^{-2} s^{-1}	1.6	1.6	1.6	1.6	1.6	1.6
"High" a	PFT-specific O_3 sensitivity parameter	$nmol^{-1}$ m^2 s	0.075	0.075	0.075	0.15	0.15	0.15
"Low" a			0.02	0.02	0.02	0.04	0.04	0.04

https://doi.org/10.5194/egusphere-2025-1375
Preprint. Discussion started: 2 April 2025

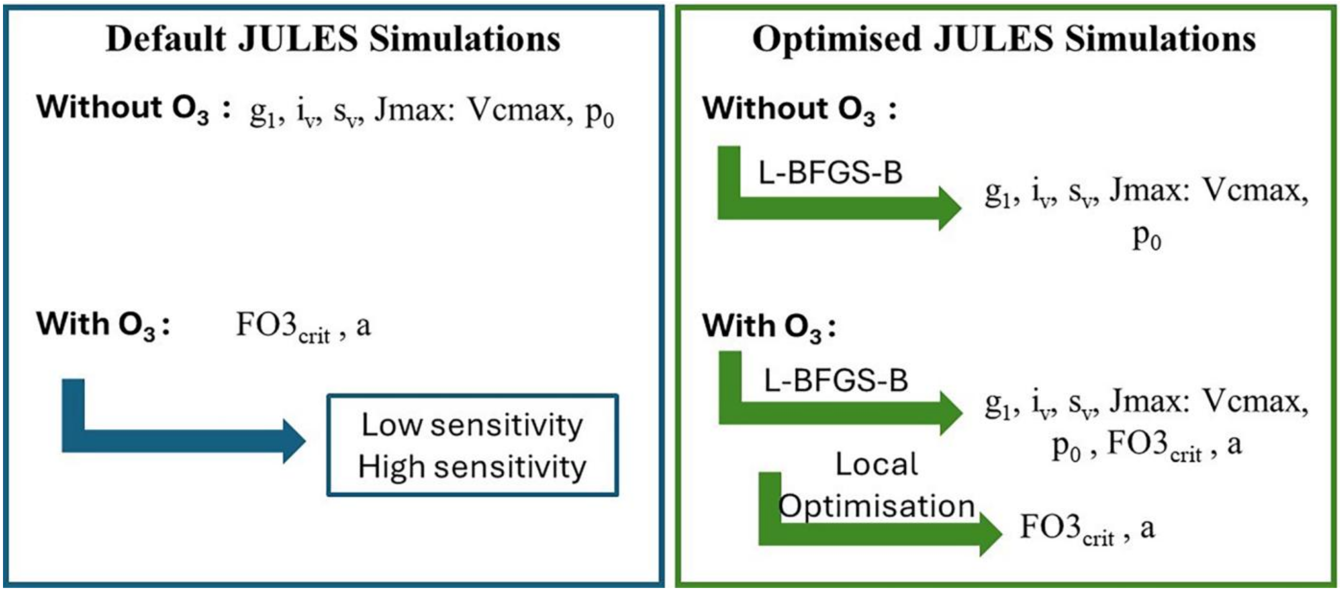

Figure 3: Overview of the two types of simulations considered in this study. Default simulations represent site-level runs with model default parameters with or without O_3 effects. Simulations with optimised parameters are also run with and without O_3 effects. For the optimised simulations without ozone, the parameters calibrated are sensitivity of stomatal conductance to the assimilation rate (g_1), the intercept (i_v) and the slope (s_v) of the linear relationship between V_{cmax} and N_a, the ratio between the carboxylation rate and the rate of electron transport at 25°C (J_{max}:V_{cmax}) and the threshold at which the plant starts to experience drought stress (p_0). For configurations with O_3, we also add the critical flux of O_3 to vegetation (F_{O3crit}) and PFT-specific O_3 sensitivity parameter (*a*).

Model evaluation

In order to evaluate the model performance, JULES was forced with the meteorology, CO_2 and O_3 observed at each site and evaluated against flux GPP data. In all simulations, the vegetation cover was prescribed using JULES default PFTs. In each simulation, phenology was simulated prognostically, allowing the model to simulate the dynamic evolution of the maximum leaf area index (LAI). Prior to running the simulations, the model underwent a 50-year spin-up phase to ensure that the model state variables were representative of steady-state conditions. We used Root Mean Squared Error (RMSE) and the coefficient of determination (r^2) to quantify the differences between the outputs from the various model simulations and the observations.

High-O_3 days analysis

To investigate the impact of elevated ozone concentrations on diurnal GPP dynamics and their interaction with latent heat (LE) and vapour pressure deficit (VPD), we analysed the temporal patterns of these variables on the days O_3 concentration is above 40 ppb for each site. Additionally, the performance of different model configurations was evaluated for these specific high-ozone days to assess their ability to capture observed GPP responses under extreme conditions.

https://doi.org/10.5194/egusphere-2025-1375
Preprint. Discussion started: 2 April 2025

2.4.3 GPP reductions due to ozone

To quantify the overall impact of O_3 on GPP, we calculated the relative reduction in GPP for each site using the optimised simulations and the configuration without O_3 impact as the baseline. This calculation was performed each year to account for interannual variability, and the results were averaged to obtain the mean relative reduction over the study period.

3 Results

3.1 Statistical Analysis: Partial correlations

The results of the partial correlation analysis highlight varying degrees of GPP sensitivity to ozone across the investigated sites (Fig. 4). Hyytiälä (FI-Hyy), Värriö (FI-Var), Brasschaat (BE-Bra), Fontainebleau-Barbeau (FR-Fon), and Bosco-Fontana (IT-BFt) exhibited consistently negative correlations between GPP and O_3, indicating a significant vulnerability to ozone pollution. The negative impact of ozone on GPP is particularly pronounced during specific conditions, such as the summer months (June, July, and August) and midday hours when radiation and temperature are high. While partial correlations control for key environmental variables such as temperature, radiation, and VPD, subsetting the dataset allows for an investigation of the residual impacts of O_3 under specific ecological conditions. These subsets, such as summer months or midday hours, represent periods of peak biological activity and potential O_3 damage, making them ecologically and practically relevant. For instance, ozone concentrations and GPP are generally higher during the summer due to increased plant activity. Subsetting ensures the analysis captures O_3 impacts under these seasonal conditions. Similarly, during midday hours, when radiation and photosynthesis peak, O_3 uptake through stomata may also reach its highest levels. This approach allows us to determine whether O_3 impacts are consistent across varying contexts or are amplified under specific conditions of heightened environmental and biological activity. Across the sites, FI-Hyy showed weak but significant negative correlations across all subsets, indicating a mild sensitivity to ozone. FI-Var exhibited slightly stronger negative correlations than FI-Hyy, particularly during midday hours in the summer, emphasising the vulnerability of boreal forest ecosystems to ozone stress under specific conditions. BE-Bra and IT-BFt demonstrated the most pronounced negative correlations during the combined summer and midday subsets, suggesting that these conditions heighten the vulnerability of these sites to ozone pollution. Notably, BE-Bra showed the strongest correlation during the summer midday period, underscoring the importance of environmental stressors in exacerbating ozone effects. FR-Fon also displayed significant negative correlations, although the magnitude was generally lower than at BE-Bra and IT-BFt, indicating a moderate sensitivity to ozone.

Conversely, the Castelporziano 2 (IT-Cp2) site exhibited a negative correlation when considering the full dataset; however, for other subsets, the correlation coefficients became positive and non-significant. This outcome may stem from the limited dataset available for IT-Cp2 and the unique characteristics of this site, including partial stomatal closure in response to drought and VPD stress during warm seasons. These factors may obscure the direct relationship between ozone and GPP at this Mediterranean site. Overall, the results emphasise the varying impacts of ozone across different environmental contexts and

https://doi.org/10.5194/egusphere-2025-1375
Preprint. Discussion started: 2 April 2025

site-specific conditions. Subsetting the data to account for periods of peak biological activity enhances our understanding of the residual effects of O_3 on GPP after controlling for other critical environmental variables. This nuanced approach provides valuable insights into the dynamics of ozone stress across diverse forest ecosystems in Europe.

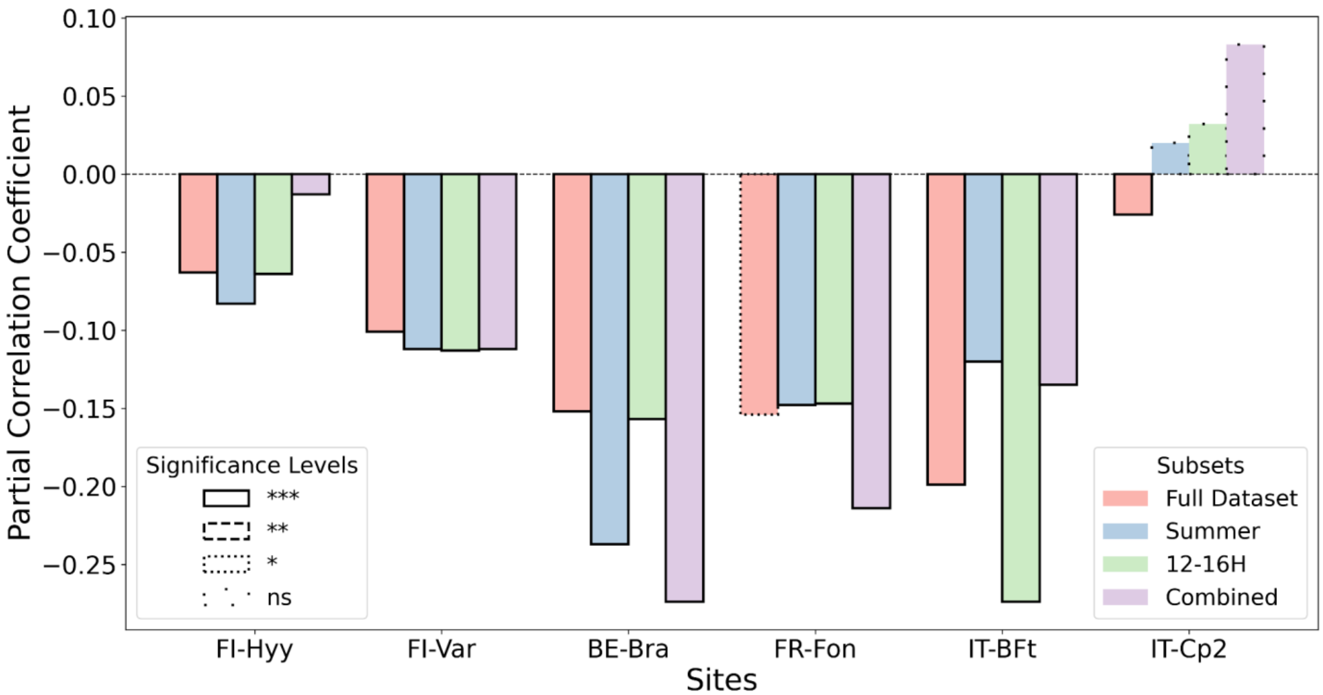

Figure 4: Partial correlation coefficients (unitless) between GPP and O_3 – after controlling for air temperature, short-wave radiation and vapour pressure deficit. The calculations were performed for all datasets (salmon bars), including summer only (blue bars, June, July, and August), midday only (green bars, 12-16H), and midday summer only (purple bars, combined). The significance levels: p-value < 0.001 ***, p-value < 0.01 **, p-value < 0.05 *, non-significant (ns).

3.2 JULES GPP simulations

The default JULES model configuration (default parameters, Table 3 and Fig. 5) generally exhibits higher variability and larger deviations from observed GPP values across all sites. The optimisation significantly improves model performance by reducing RMSE and increasing r^2 values across most sites (Table 3). However, the incorporation of O_3 effects yields mixed results, with improvements in RMSE at certain sites (e.g., FR-Fon, IT-BFt) but little to no improvement at others, such as FI-Hyy and BE-Bra (Table 3).

At FI-Hyy, both default and optimised models perform well, with slight improvements in RMSE and r^2 following optimisation. The optimised simulation with O_3 achieves the greatest reduction in RMSE (2.11 µmol CO_2 m^{-2} s^{-1}) and an increase in r^2

https://doi.org/10.5194/egusphere-2025-1375
Preprint. Discussion started: 2 April 2025

(0.86). These improvements reflect the model's ability to adjust to local conditions with minimal parameter changes (Fig. 6), particularly in boreal settings. However, the inclusion of O_3 does not significantly alter RMSE, suggesting that GPP at this site is not highly sensitive to ozone stress. At FI-Var, optimisation reduces underestimations during midday peaks and aligns simulated GPP with observations. Therefore, the optimised configuration achieves a 1.65 μmol CO_2 m^{-2} s^{-1} RMSE and 0.75 r^2. Key parameter adjustments, such as increases in g_1 and decreases in p_0 (Figs. 6a and 6e), contribute to these improvements. Incorporation of O_3 effects only slightly improves RMSE at FI-Var, suggesting moderate sensitivity to ozone impacts at this boreal site.

At BE-Bra, the default configuration performs well, and optimisation further reduces RMSE and improves r^2. The optimised simulation achieves an RMSE of 3.36 μmol CO_2 m^{-2} s^{-1} and an r^2 of 0.81, highlighting the importance of fine-tuning parameters such as g_1 and s_v (Figs. 6a and 6d). However, the inclusion of O_3 has a minimal impact on RMSE at this site, suggesting relatively low ozone sensitivity compared to other locations. At FR-Fon, default simulations significantly underestimate GPP during peak hours, especially under high ozone stress. The optimisation improves model accuracy, showing a reduction in RMSE (5.71 μmol CO_2 m^{-2} s^{-1}) and an increase in r^2 (0.60). Despite these improvements, some underestimation remains, indicating that additional refinement of O_3 response mechanisms or GPP modelling may be needed at this site.

At IT-BFt, the default model exhibits large variability in GPP, reflecting the challenges of modeling Mediterranean ecosystems. The optimised configuration achieves the greatest improvements, reducing RMSE to 3.78 μmol CO_2 m^{-2} s^{-1} and increasing r^2 to 0.82. Adjustments to $FO3_{crit}$, *a*, and p_0 (Fig. 6f, 6g, and 6e) enhance performance by addressing both ozone and water stress, highlighting the strong impact of O_3 at this site. At IT-Cp2, the default model underestimates GPP during midday peaks, particularly under ozone stress. The optimised configuration achieves the best results, reducing RMSE to 2.85 μmol CO_2 m^{-2} s^{-1} and increasing r^2 to 0.72. Adjustments to $FO3_{crit}$ and *a* play a critical role in capturing ozone impacts at this Mediterranean site, demonstrating the necessity of refining these parameters in high-ozone environments.

Overall, parameter optimisation improves model accuracy and reliability across all sites. However, the inclusion of O_3 effects leads to site-specific responses, with improvements in RMSE at some sites (e.g., FR-Fon, IT-BFt) but minimal changes in r^2 across most locations. Figure 5 highlights that in some cases, the addition of O_3 increases model biases, despite RMSE values suggesting only slight degradation in performance. These findings underscore the need for continued refinement of ozone response mechanisms to improve model accuracy, particularly in Mediterranean regions where ozone exposure and water stress are strongly coupled.

Table 3: Summary of model evaluation metrics: root mean square error (RMSE, μmol CO_2 m^{-2} s^{-1}) and coefficient of determination (r^2) values for each site. The metrics are calculated for default and optimised simulations with and without ozone impacts.

	FI-Hyy	FI-Var	BE-Bra	FR-Fon	IT-BFt	IT-Cp2
Default						

https://doi.org/10.5194/egusphere-2025-1375
Preprint. Discussion started: 2 April 2025

Metrics	**RMSE**	**r^2**	**RMSE**	**r^2**	**RMSE**	**r^2**	**RMSE**	**r^2**	**RMSE**	**r^2**	**RMSE**	**r^2**
Without O_3	2.88	0.83	3.87	0.63	4.06	0.76	9.53	0.39	6.30	0.53	3.81	0.65
With O_3	2.85	0.83	3.08	0.65	3.97	0.77	8.85	0.48	5.78	0.60	3.73	0.69
Optimised												
Metrics	**RMSE**	**r^2**	**RMSE**	**r^2**	**RMSE**	**r^2**	**RMSE**	**r^2**	**RMSE**	**r^2**	**RMSE**	**r^2**
Without O_3	2.88	0.83	2.41	0.73	3.92	0.77	8.72	0.49	4.35	0.75	3.69	0.70
With O_3	2.11	0.86	1.65	0.75	3.36	0.81	5.71	0.60	3.78	0.82	2.85	0.72

https://doi.org/10.5194/egusphere-2025-1375
Preprint. Discussion started: 2 April 2025

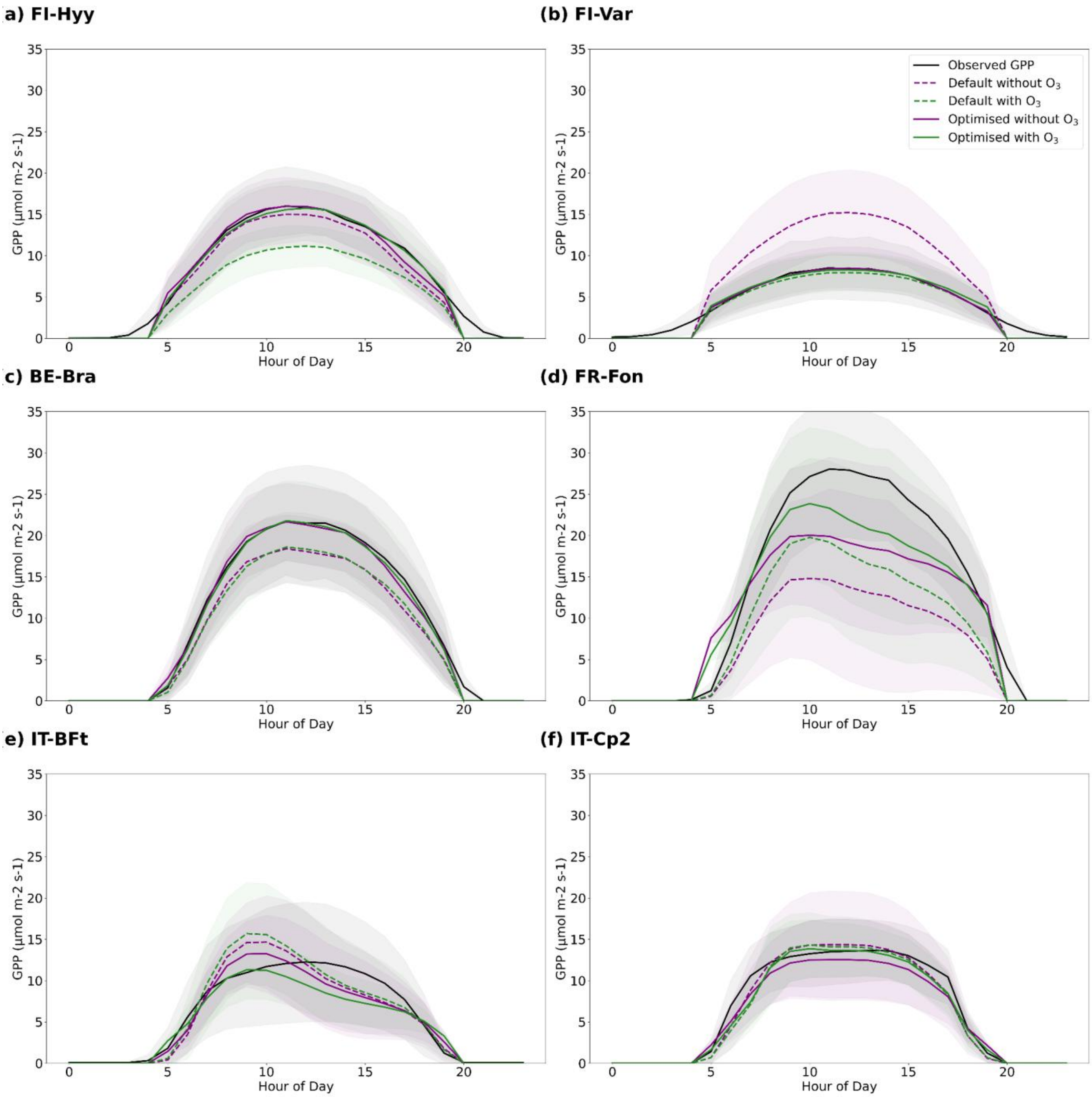

Figure 5: Comparison of the observed and simulated GPP diurnal cycles across all sites: (a) FI-Hyy, (b) FI-Var, (c) BE-Bra, (d) FR-Fon, (e) IT-BFt and (f) IT-Cp2. Shaded areas encompass plus and minus one standard deviation. The black line represents the observed GPP. The default simulated GPP are the dashed purple line (without O_3) and dashed green line (with O_3), and optimised simulated GPP are the purple line (without O_3) and green line (with O_3).

https://doi.org/10.5194/egusphere-2025-1375
Preprint. Discussion started: 2 April 2025

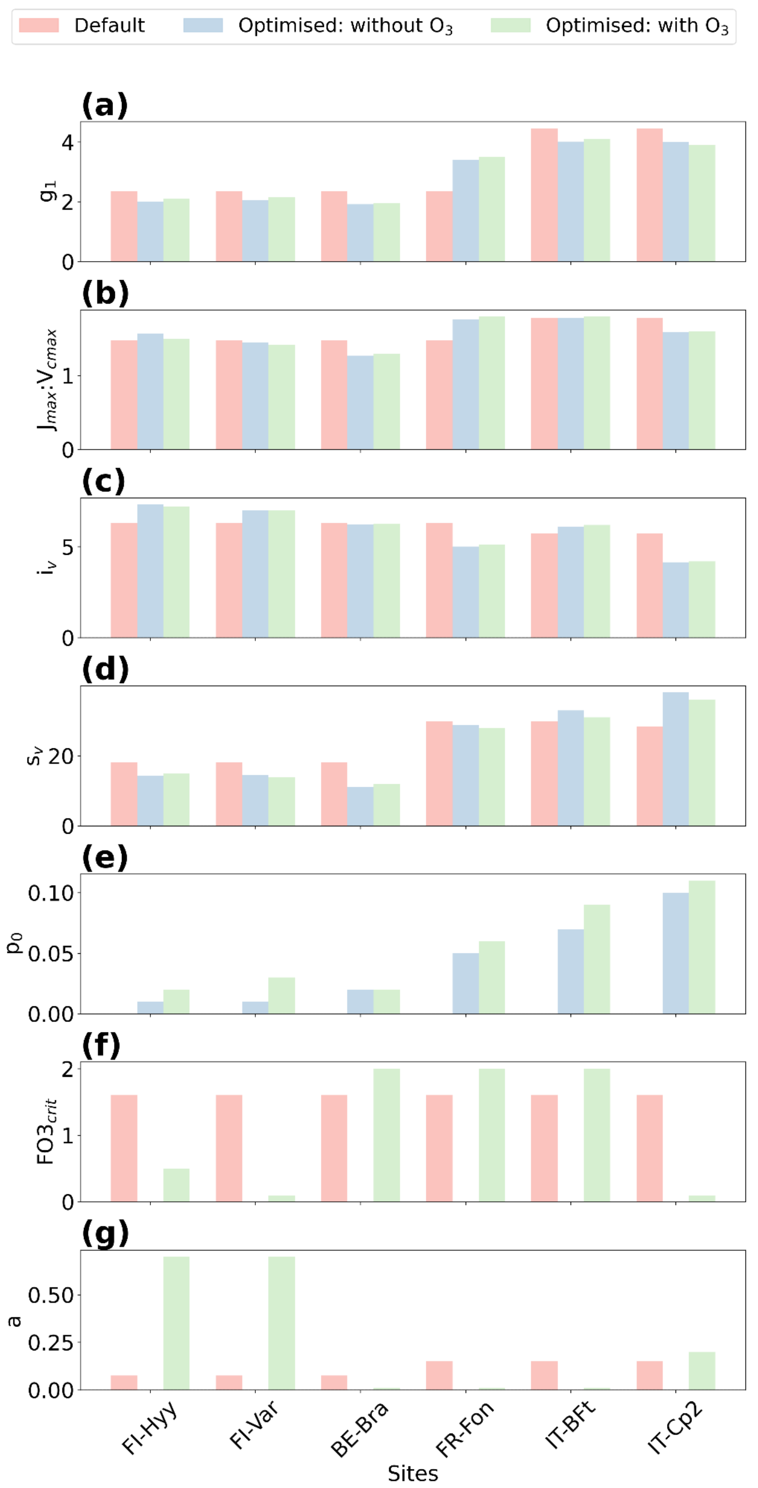

367

https://doi.org/10.5194/egusphere-2025-1375
Preprint. Discussion started: 2 April 2025

Figure 6: Comparison of default and optimised parameters. The figure presents a comparison between the default (salmon bars) and optimised parameter values: without ozone (blue bars) and with ozone (green bars) for the six sites. The parameters include (a) stomatal conductance sensitivity to assimilation rate (g_1), (b) the ratio of maximum potential electron transport rate to maximum carboxylation rate (J_{max}:V_{cmax}), (c) and (d) parameters related to leaf nitrogen (i_v and s_v), (e) soil moisture stress threshold (p_0), (f) the critical ozone flux ($FO3_{crit}$), and (g) the sensitivity parameter (*a*).

3.3 Interaction of O_3 with environmental factors on GPP during high ozone days

For high O_3 days (above 40 ppb), across all sites, the observed GPP shows a characteristic peak around midday, with simulated GPP that includes O_3 effects generally aligning more closely with the observed data compared to simulations that exclude O_3 effects (Fig. 7). However, the magnitude of this improvement varies by site.

Ozone concentrations follow a diurnal cycle, peaking in the afternoon (12:00–16:00) across all sites. This peak reflects the influence of high solar radiation, temperature, and atmospheric dynamics. The impact of O_3 on GPP is modulated by interactions with key environmental factors such as vapour pressure deficit (VPD) and latent heat flux (LE), both of which influence stomatal conductance. When VPD and LE peak around midday, stomatal conductance typically increases, facilitating greater O_3 uptake and intensifying its effects on photosynthesis.

At boreal sites (FI-Hyy and FI-Var), ozone peaks reach moderate levels (~46 and 44 ppb, respectively), yet their impact on GPP appears limited. FI-Var, in particular, shows minimal reductions in GPP, suggesting that this site is relatively resilient to ozone stress. This is reflected in the small RMSE improvement (3.10 to 1.18 µmol CO_2 m^{-2} s^{-1}, Table 4) when incorporating O_3 effects. At FI-Hyy, however, simulations without O_3 significantly underestimate GPP, leading to a high RMSE (9.97 µmol CO_2 m^{-2} s^{-1}), which improves dramatically when O_3 effects are included (RMSE = 0.52 µmol CO_2 m^{-2} s^{-1}). This suggests that while FI-Hyy is less sensitive to O_3 overall, proper parameterisation of O_3 effects improves model performance.

At BE-Bra, GPP reductions due to ozone are more pronounced, with RMSE dropping from 7.57 to 3.09 µmol CO_2 m^{-2} s^{-1} when O_3 effects are considered. This improvement highlights the need to include ozone stress in GPP simulations, particularly in temperate forests where stomatal ozone uptake remains substantial. Interestingly, at FR-Fon, while ozone peaks coincide with midday GPP declines, the difference between with and without O_3 simulations is small in Figure 7. This is confirmed by the minor RMSE reduction (5.60 to 5.47 µmol CO_2 m^{-2} s^{-1}, Table 4), suggesting that other factors—such as phenology or local climate conditions—play a dominant role in regulating GPP at this site.

Mediterranean sites (IT-BFt and IT-Cp2) experience the highest ozone peaks (>60 ppb), which coincide with sharper midday declines in GPP. Unlike boreal and temperate sites, where O_3 effects were moderate, these ecosystems exhibit stronger O_3-induced reductions in GPP. At IT-Cp2, including O_3 in the model reduces RMSE from 5.45 to 1.93 µmol CO_2 m^{-2} s^{-1}, the most significant improvement across all sites. Similarly, at IT-BFt, RMSE drops from 5.88 to 2.31 µmol CO_2 m^{-2} s^{-1}. These reductions highlight the necessity of incorporating O_3 stress in Mediterranean regions, where high VPD and stomatal conductance increase ozone uptake, amplifying physiological stress.

Interestingly, despite the strong midday declines in GPP at Mediterranean sites, Figure 6 suggests that the ozone sensitivity parameters are generally lower in Mediterranean forests. This indicates that the observed ozone effects in these regions are primarily driven by higher ambient O_3 concentrations rather than an inherently higher sensitivity of Mediterranean vegetation.

https://doi.org/10.5194/egusphere-2025-1375
Preprint. Discussion started: 2 April 2025

Overall, these results reinforce the importance of including O_3 effects in GPP simulations, particularly in regions with high ozone exposure. While boreal sites show limited O_3 sensitivity, temperate and Mediterranean forests experience stronger reductions, necessitating careful model calibration to capture these interactions. The combination of ozone stress, VPD, and latent heat flux (LE) amplifies these effects, further emphasising the need for site-specific parameter tuning.

Table 4: Performance of optimised JULES without O_3 and with O_3 for O_3 levels above 40 ppb for each site.

	FI-Hyy		FI-Var		BE-Bra		FR-Fon		IT-BFt		IT-Cp2	
Metrics	RMSE	r^2	RMSE	r^2	RMSE	r^2	RMSE	r^2	RMSE	r^2	RMSE	r^2
Without O_3	9.97	0.46	3.10	0.65	7.57	0.60	5.60	0.55	5.88	0.42	5.45	0.70
With O_3	0.52	0.85	1.18	0.70	3.09	0.73	5.47	0.59	2.31	0.65	1.93	0.77

https://doi.org/10.5194/egusphere-2025-1375
Preprint. Discussion started: 2 April 2025

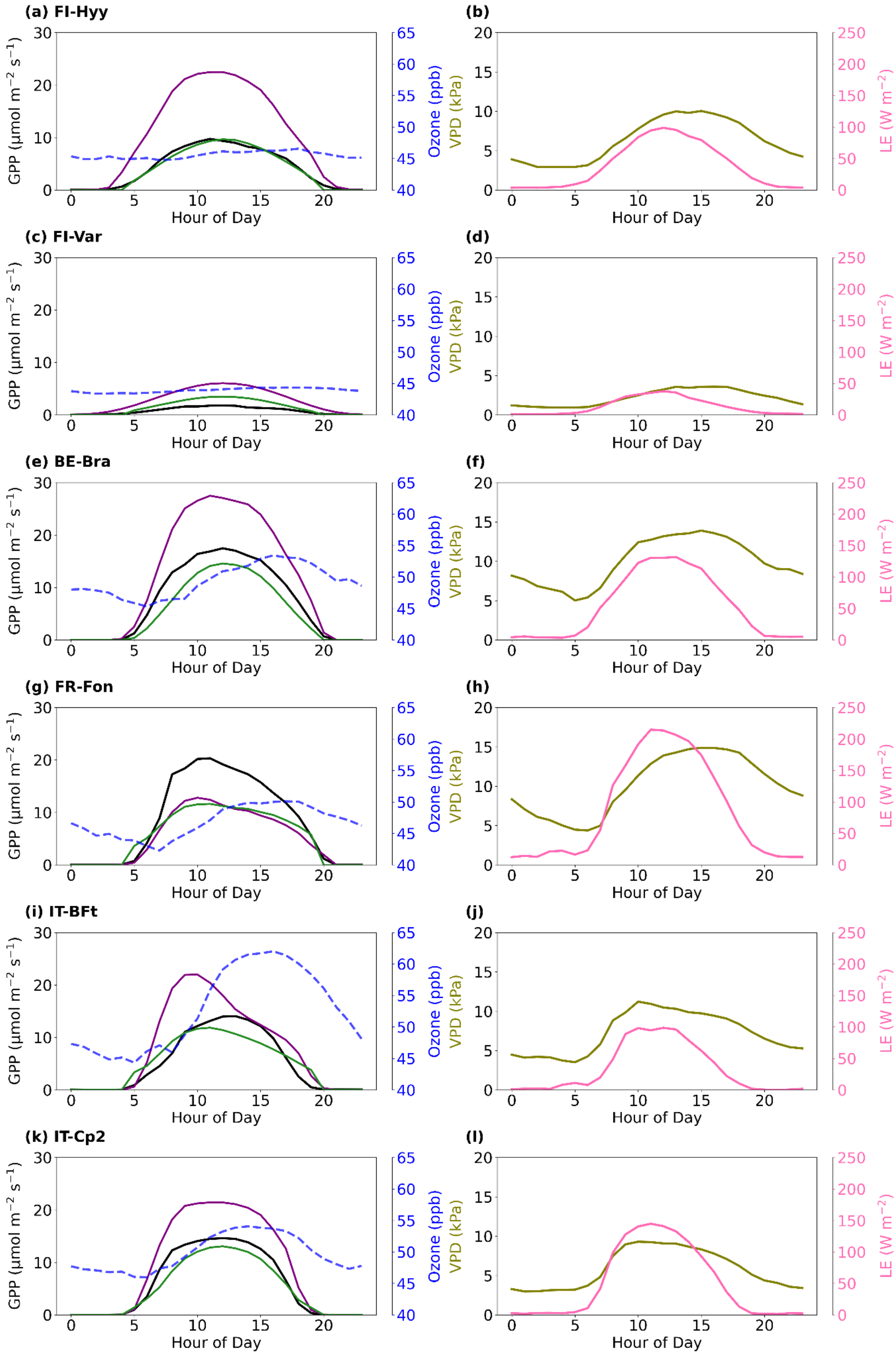

https://doi.org/10.5194/egusphere-2025-1375
Preprint. Discussion started: 2 April 2025

Figure 7: Averaged diurnal cycles of GPP, ozone (O_3), vapour pressure deficit (VPD), and latent heat (LE) across sites on days when ozone levels exceeded 40 ppb: (a, b) FI-Hyy, (c, d) FI-Var, (e, f) BE-Bra, (g, h) FR-Fon, (i, j) IT-BFt, and (k, l) IT-Cp2, showing the observed (black line) and optimised simulated GPP without O_3 (purple line) and with O_3 (green), O_3 concentration (Ozone, blue) at left column and vapour pressure deficit (VPD, olive), and latent heat flux (LE, pink) on the right column.

3.4 GPP reductions due to O_3 effects

The mean annual GPP reduction varies significantly across the sites, suggesting a site-specific exposure and response to ozone stress (Fig. 8). The negative values indicate a decrease in GPP, highlighting the impact of ozone as a stressor on plant productivity.

FI-Hyy and FI-Var show relatively small reductions in GPP, with annual mean decreases of -1.36 % and -1.04 %, respectively. This suggests that these northern sites are less sensitive to ozone stress, possibly due to lower background O_3 concentrations (Fig. 2, Table 1) or lower stomatal ozone uptake, which limits the damaging effects on GPP. In contrast, IT-BFt and IT-Cp2 exhibit the highest reductions (-6.2% and -5.4%, respectively), which can be attributed to higher ozone exposure (Fig. 2) and greater ozone uptake, exacerbating stress on photosynthesis and stomatal function. Similarly, temperate forests (BE-Bra and FR-Fon) exhibit moderate reductions in GPP, with declines of 5.22% and -2.62%, respectively. While ozone effects at FR-Fon are lower than those at BE-Bra, they are still significant, underscoring that broadleaf deciduous forests also experience ozone-induced productivity losses. The stronger impact at BE-Bra may be linked to higher stomatal ozone uptake, as suggested by the site's parameter sensitivity (Fig. 6).

These findings highlight the need for region-specific ozone mitigation strategies, particularly in Mediterranean ecosystems where ozone-induced reductions in GPP exceed 5% annually. The combination of high ozone, VPD, and water stress in these regions may further amplify productivity losses, making them particularly vulnerable to future climate and air quality changes.

https://doi.org/10.5194/egusphere-2025-1375
Preprint. Discussion started: 2 April 2025

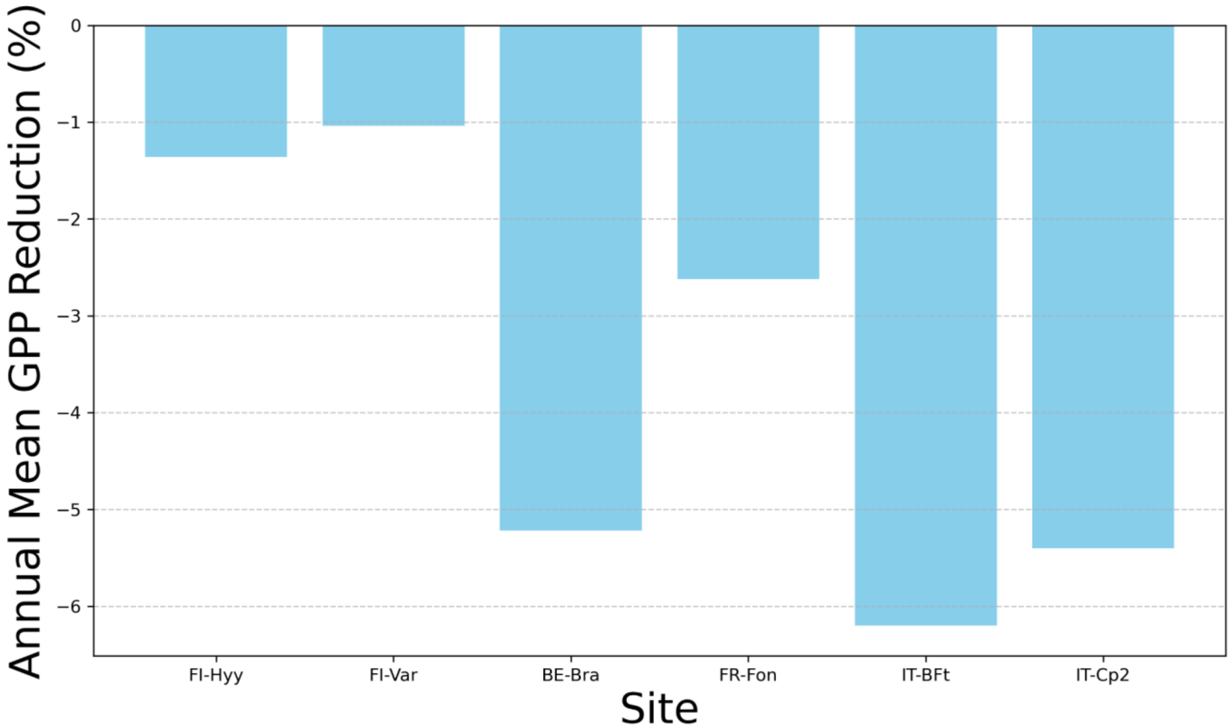

Figure 8: Annual mean GPP reduction due to ozone exposure (%). The bar plot represents the annual mean reduction in Gross Primary Productivity (GPP) as a percentage for each site: FI-Hyy, FI-Var, BE-Bra, FR-Fon, IT-BFt, and IT-Cp2.

4 Discussion and Conclusions

This study underscores the importance of incorporating ozone effects into the JULES model to enhance its accuracy in simulating Gross Primary Productivity (GPP) across diverse European forest ecosystems. By including ozone effects, the model demonstrated improved performance, particularly during high O_3 events and in central and southern European sites where ozone stress is most pronounced. For example, reductions in RMSE at FR-Fon (from 9.53 to 5.71), IT-BFt (from 6.30 to 3.78), and IT-Cp2 (from 3.81 to 2.85) highlight the significant role of ozone in modulating plant productivity. These findings confirm previous observations that ozone exposure strongly influences plant photosynthesis and carbon sequestration, particularly in Mediterranean climates (Sitch et al., 2007). However, the minimal differences in northern European sites (FI-Hyy and FI-Var) suggest boreal forests' lower sensitivity to ozone, aligning with prior research showing lower ozone uptake in cooler, high-latitude environments (Wittig et al., 2009). The annual mean GPP reductions due to ozone exposure reveal a clear spatial gradient, with northern sites showing minimal reductions (-1.04% to -1.36%) and southern sites experiencing more pronounced decreases (-5.4% to -6.2%). This gradient reflects the interplay of higher ambient ozone concentrations, greater stomatal conductance, and compounding environmental stressors such as high temperatures and vapor pressure deficit in Mediterranean climates (Proietti et al., 2016). Central European sites (e.g., BE-Bra and FR-Fon) exhibited intermediate

https://doi.org/10.5194/egusphere-2025-1375
Preprint. Discussion started: 2 April 2025

reductions, consistent with transitional climatic conditions that modulate ozone impacts. These patterns emphasise the importance of considering regional climatic variables in modeling ozone effects on GPP. For instance, Mediterranean species often exhibit adaptations such as enhanced antioxidant production to mitigate ozone damage, though these defenses can be overwhelmed under extreme environmental stress.

A key insight from our study is the potential overestimation of ozone impacts in prior modeling efforts. For example, Anav et al. (2011) estimated a 22% reduction in annual GPP across Europe using the ORCHIDEE model, while Oliver et al. (2018) simulated that GPP was reduced by 10 to 20% in temperate regions and by 2 to 8% in boreal regions using JULES. These discrepancies likely stem from differences in the resolution and accuracy of ozone and GPP datasets. By integrating high-resolution in situ ozone, meteorology, and GPP measurements, our study provides more precise estimates, reducing the biases inherent in purely simulation-based approaches. For instance, Gerosa et al. (2022) reported GPP reductions of 2.93% to 6.98% at IT-BFt using statistical models based on in situ data, aligning closely with our findings of a -6.2% GPP reduction. Similar conclusions were found by Conte et al. (2021), who adopted statistical models based on dynamic seasonal thresholds of ozone doses to reduce the bias between observed and modelled GPP. These results highlight the critical role of empirical data in refining model predictions.

This study's diurnal GPP, ozone, VPD, and LE patterns provide additional insights into the interaction between ozone and environmental stressors. Across all sites, ozone concentrations peaked in the late afternoon, coinciding with periods of high VPD and LE. This temporal alignment underscores the role of atmospheric conditions—such as high solar radiation and temperatures—in driving ozone formation and stomatal ozone uptake. Southern sites like IT-BFt and IT-Cp2 exhibited pronounced midday declines in GPP, reflecting their heightened sensitivity to ozone and the compounding effects of high VPD and LE. These findings align with the work of Ainsworth et al. (2012), who demonstrated that multiple stressors can exacerbate the physiological impacts of ozone on plants.

In contrast, boreal sites such as FI-Hyy exhibited minimal midday GPP reductions, consistent with their relative resilience to ozone stress under cooler atmospheric conditions. This supports prior research suggesting that boreal species often operate under a narrower range of stomatal conductance, limiting ozone uptake even during peak stress periods (Hoshika et al., 2013, Rannik et al., 2012). The variability in ozone impacts across sites emphasises the need for regional calibration of land surface models like JULES. This study optimised key parameters—including the critical ozone flux, stomatal conductance sensitivity, and ozone sensitivity coefficient- to improve model performance. However, discrepancies at specific sites, such as FR-Fon and IT-Cp2, indicate that further refinement is necessary to capture local environmental conditions.

Our study highlights the importance of integrating long-term in situ measurements into land surface models to improve their accuracy and reliability. Expanding such measurements' spatial and temporal coverage is essential for capturing the full variability of ozone impacts across biomes and climatic conditions. Future research should also prioritise refining ozone response mechanisms in land surface models, particularly in regions where multiple stressors interact to influence plant productivity. For example, incorporating dynamic responses to heat waves, droughts, and other extreme events could provide a more comprehensive understanding of how ozone stress interacts with climate change.

Code Availability

JULES-vn7.4 was used for all simulations. The JULES model code and suite used to run the model are available from the Met Office Science Repository Service (MOSRS). Registration is required, and the code is available to anyone for non-commercial use (for details of licensing, see https://jules.jchmr.org/code, last access: 29 June 2024). Visit the JULES website (https://jules.jchmr.org/getting-started, last access: 29 June 2024) to register for a MOSRS account. Documentation for the JULES model is located at https://jules-lsm.github.io/vn7.4/ (last access: 29 June 2024). Site-level simulations used the rose suite u-dg903 (https://code.metoffice.gov.uk/trac/roses-u/browser/d/g/9/0/3, at revision 289677), which is a copy of the u-al752 JULES suite for FLUXNET 2015 and LBA sites described at https://code.metoffice.gov.uk/trac/jules/wiki/FluxnetandLbaSites (last access: 29 June 2024) and downloaded from https://code.metoffice.gov.uk/trac/roses-u/browser/a/l/7/5/2/ (Harper et al., 2021) at revision 286601. Suites can be downloaded from MOSRS once the user has registered for an account.

Data Availability

The ICOS data (meteorological variables, fluxes and carbon dioxide concentration) used to run JULES are available for download from https://www.icos-cp.eu/observations (last access: 29 June 2024). The ozone data was obtained by requesting the PIs of each site, except Värriö, obtained through the SMEAR I research station (Kolari et al., 2024) and Hyytiälä, available on SMEAR II Hyytiälä forest meteorology, greenhouse gases, air quality and soil dataset (Aalto et al., 2023).

Author contribution

IV wrote the paper and led the data analysis, with contributions from all authors. FM, SS, FB, PB, MB and HV contributed to the interpretation of the data. GG and SF contributed to in situ data for model evaluation. MCDR, SS and FB contributed to JULES simulations.

Competing interests

At least one of the (co-)authors is a member of the editorial board of Biogeosciences.

Acknowledgements

IV was funded by Fonds Wetenschappelijk Onderzoek Flanders (FWO grant no. G018319N). FM was funded by the FWO as a senior postdoc and is thankful to this organisation for its financial support (FWO grant no. 1214723N). SS was funded through UKRI NERC funding (NE/R001812/1). MCDR has been supported by the H2020 4C project no. 821003, by the

NetZeroPlus (NZ+) grant funded by UKRI-BBSRC award BB/V011588/1 and also by the UKRI-'AI for Net Zero' Programme project: ADD-TREES, Grant number EP/Y005597/1. The authors acknowledge Ivan Jansens from the University of Antwerp and Daniel Berveiller from the University of Paris-Saclay for the ozone datasets provided for the Brasschaat and Fontainebleau-Barbeau sites, respectively.

References

Aalto, J., Aalto, P., Keronen, P., Kolari, P., Rantala, P., Taipale, R., Kajos, M., Patokoski, J., Rinne, J., Ruuskanen, T., Leskinen, M., Laakso, H., Levula, J., Pohja, T., Siivola, E., Kulmala, M., & Ylivinkka, I.: SMEAR II Hyytiälä forest meteorology, greenhouse gases, air quality and soil. University of Helsinki, Institute for Atmospheric and Earth System Research. https://doi.org/10.23729/23dd00b2-b9d7-467a-9cee-b4a122486039, 2023.

Ainsworth, E. A., Lemonnier, P., and Wedow, J. M.: The influence of rising tropospheric carbon dioxide and ozone on plant productivity, Plant Biol., 21, 59-71, 2019.

Ainsworth, E. A., Yendrek, C. R., Sitch, S., Collins, W. J., and Emberson, L. D.: The effects of tropospheric ozone on net primary productivity and implications for climate change, Annu. Rev. Plant Biol., 63, 637-661, 2012.

Anav, A., Menut, L., Khvorostyanov, D., and Viovy, N.: Impact of tropospheric ozone on the Euro-Mediterranean vegetation, Glob. Change Biol., 17, 2342–2359, https://doi.org/10.1111/j.1365-2486.2010.02387.x, 2011.

Anav, A., De Marco, A., Proietti, C., Alessandri, A., Dell'Aquila, A., Cionni, I., Friedlingstein, P., Khvorostyanov, D., Menut, L., Paoletti, E., Sicard, P., Sitch, S., & Vitale, M.: Comparing concentration-based (AOT40) and stomatal uptake (PODY) metrics for ozone risk assessment to European forests, Global Change Biology, 22, https://doi.org/10.1111/gcb.13138, 2016.

Best, M. J., Pryor, M., Clark, D. B., Rooney, G. G., Essery, R. L. H., Ménard, C. B., Edwards, J. M., Hendry, M. A., Porson, A., Gedney, N., Mercado, L. M., Sitch, S., Blyth, E., Boucher, O., Cox, P. M., Grimmond, C. S. B., and Harding, R. J.: The Joint UK Land Environment Simulator (JULES), model description – Part 1: Energy and water fluxes, Geosci. Model Dev., 4, 677–699, https://doi.org/10.5194/gmd-4-677-2011, 2011.

Cailleret, M., Ferretti, M., Gessler, A., Rigling, A., & Schaub, M.: Ozone effects on European forest growth—Towards an integrative approach, Journal of Ecology, 106, 1377 - 1389. https://doi.org/10.1111/1365-2745.12941, 2018.

Clark, D. B., Mercado, L. M., Sitch, S., Jones, C. D., Gedney, N., Best, M. J., Pryor, M., Rooney, G. G., Essery, R. L. H., Blyth, E., Boucher, O., Harding, R. J., Huntingford, C., and Cox, P. M.: The Joint UK Land Environment Simulator (JULES), model description – Part 2: Carbon fluxes and vegetation dynamics, Geosci. Model Dev., 4, 701–722, https://doi.org/10.5194/gmd-4-701-2011, 2011.

Clifton, O. E., Fiore, A. M., Correa, G., Horowitz, L. W., and Naik, V.: Effects of regional climate change on air quality across the United States: a review of dynamic modeling studies, Environ. Res. Lett., 15, 123007, 2020.

Conte, A., Otu-Larbi, F., Alivernini, A., Hoshika, Y., Paoletti, E., Ashworth, K., & Fares, S.: Exploring new strategies for ozone-risk assessment: A dynamic-threshold case study. Environmental Pollution, 287, 117620. https://doi.org/10.1016/j.envpol.2021.117620, 2021.

Dengel, S., Grace, J., Aakala, T., Hari, P., Newberry, S. L., and Mizunuma, T.: Spectral characteristics of pine needles at the limit of tree growth in subarctic Finland, Plant Ecol. Divers., 6**,** 31–44, https://doi.org/10.1080/17550874.2012.754512, 2013.

Ducker, J., Muller, J. B., Whalley, L. K., Parker, A. E., and Oetjen, H.: The impact of leaf physiology on the ozone flux of an urban woodland, Agric. For. Meteorol., 252, 51-63, 2018.

Emberson, L. D., Ashmore, M. R., Cambridge, H. M., Simpson, D., and Tuovinen, J. P.: Modelling stomatal ozone flux across Europe, Water Air Soil Pollut., 130, 577-582, 2001.

Farquhar, G. D., von Caemmerer, S., and Berry, J. A.: A biochemical model of photosynthetic CO_2 assimilation in leaves of C_3 species, Planta, 149, 78–90, https://doi.org/10.1007/BF00386231, 1980.

Feng, Z., Xu, Y., Kobayashi, K., Dai, L., Zhang, T., Agathokleous, E., Calatayud, V., Paoletti, E., Mukherjee, A., Agrawal, M., Park, R. J., Oak, Y. J., and Yue, X.: Ozone pollution threatens the production of major staple crops in East Asia, Nat. Food, 3, 47–56, https://doi.org/10.1038/s43016-021-00422-6, 2022.

Fowler, D., Coyle, M., Skiba, U., Sutton, M. A., Cape, J. N., Reis, S., Sheppard, L. J., Jenkins, A., Grizzetti, B., Galloway, J. N., Vitousek, P., Leach, A., Bouwman, A. F., Butterbach-Bahl, K., Dentener, F., Stevenson, D., Amann, M., and Voss, M.: The global nitrogen cycle in the twenty-first century, Philos. Trans. R. Soc. B Biol. Sci., 368, 20130164, 2009.

Gerosa, G. A., Marzuoli, R., and Finco, A.: Interannual variability of ozone fluxes in a broadleaf deciduous forest in Italy, Elementa: Sci. Anthrop., 10(1), doi:10.1525/elementa.2021.00105, 2022.

Gielen, B., Vandermeiren, K., Serneels, R., Valcke, R., and Ceulemans, R.: Ozone stress in young trees: Effects on photosynthesis, leaf area and root biomass allocation, Tree Physiol., 27, 123-131, 2007.

Gratani, L., and Crescente, M. F.**:** Map-making of plant biomass and leaf area index for management of protected areas, *Aliso: A Journal of Systematic and Floristic Botany*, 19, 13–24, https://scholarship.claremont.edu/aliso/vol19/iss1/2, 2000.

Grulke, N., & Heath, R.: Ozone effects on plants in natural ecosystems. Plant biology, https://doi.org/10.1111/plb.12971, 2019.

Harper, A. B., Cox, P. M., Friedlingstein, P., Wiltshire, A. J., Jones, C. D., Sitch, S., Mercado, L. M., Groenendijk, M., Robertson, E., Kattge, J., Bönisch, G., Atkin, O. K., Bahn, M., Cornelissen, J., Niinemets, Ü., Onipchenko, V., Peñuelas, J., Poorter, L., Reich, P. B., Soudzilovskaia, N. A., and Bodegom, P. V.: Improved representation of plant functional types and physiology in the Joint UK Land Environment Simulator (JULES v4.2) using plant trait information, Geosci. Model Dev., 9, 2415–2440, https://doi.org/10.5194/gmd-9-2415-2016, 2016.

Harper, A. B., Williams, K. E., McGuire, P. C., Duran Rojas, M. C., Hemming, D., Verhoef, A., Huntingford, C., Rowland, L., Marthews, T., Breder Eller, C., Mathison, C., Nobrega, R. L. B., Gedney, N., Vidale, P. L., Otu-Larbi, F., Pandey, D., Garrigues, S., Wright, A., Slevin, D., De Kauwe, M. G., Blyth, E., Ardö, J., Black, A., Bonal, D., Buchmann, N., Burban, B., Fuchs, K., de Grandcourt, A., Mammarella, I., Merbold, L., Montagnani, L., Nouvellon, Y., Restrepo-Coupe, N., and Wohlfahrt, G.: Improvement of modeling plant responses to low soil moisture in JULESvn4.9 and evaluation against flux tower measurements, Geosci. Model Dev., 14, 3269–3294, https://doi.org/10.5194/gmd-14-3269-2021, 2021.

Harper, A., Williams, K., McGuire, P. C., Duran Rojas, C., and Otu-Larbi, F.: Rose suite u-al752, MetOffice [code], https://code.metoffice.gov.uk/trac/roses-u/browser/a/l/7/5/2/trunk, last access: 29 June 2024.

Hoshika, Y., Watanabe, M., Inada, N., & Koike, T.: Model-based analysis of avoidance of ozone stress by stomatal closure in Siebold's beech (Fagus crenata).. Annals of botany, 112 6, 1149-58 . https://doi.org/10.1093/aob/mct166, 2013.

Hoshika, Y., Fares, S., Pellegrini, E., Conte, A., & Paoletti, E.: Water use strategy affects avoidance of ozone stress by stomatal closure in Mediterranean trees -A modelling analysis, Plant, cell & environment, https://doi.org/10.1111/pce.13700, 2019;

Jarvis, P. G.: The interpretation of the variations in leaf water potential and stomatal conductance found in canopies in the field, Philos. Trans. R. Soc. Lond. B Biol. Sci., 273, 593-610, 1976.

Kangasjarvi, J., Jaspers, P., Kollist, H., and Brosche, M.: Mechanisms of plant responses to ozone, Biol. Plant., 49, 5-19, 2005.

Kolari, P., Dengel, S., Peltola, O., Sahoo, G., & Siivola, E.: SMEAR I Värriö forest eddy covariance. University of Helsinki, Institute for Atmospheric and Earth System Research. https://doi.org/10.23729/6dd3e1bf-22f3-4f83-aed3-a39da5181d29, 2024.

Li, P., Feng, Z., and Paoletti, E.: A meta-analysis on growth, physiological, and biochemical responses of woody species to tropospheric ozone, Environ. Pollut., 244, 322-331, 2019.

Li, Y., Zhang, W., Wang, X., and Tian, Y.: Effects of ozone on carbon cycling and sequestration in terrestrial ecosystems: A review, Sci. Total Environ., 838, 156316, 2022.

Lombardozzi, D., Levis, S., Bonan, G., and Sparks, J. P.: Predicting photosynthesis and transpiration responses to ozone: decoupling modeled photosynthesis and stomatal conductance, Biogeosciences, 9, 3113–3130, https://doi.org/10.5194/bg-9-3113-2012, 2012.

Lombardozzi, D., S. Levis, G. Bonan, P. G. Hess, and J. P. Sparks, 2015: The Influence of Chronic Ozone Exposure on Global Carbon and Water Cycles. J. Climate, 28, 292–305, https://doi.org/10.1175/JCLI-D-14-00223.1.

Lu, J., Yao, L.: Observational evidence for detrimental impact of inhaled ozone on human respiratory system. BMC Public Health 23, 929 , https://doi.org/10.1186/s12889-023-15902-6, 2023

Lu, X., Zhang, L., and Chen, Y.: Interactions between urbanisation, economic development and air pollution in China: Evidence from dynamic simultaneous equations models, J. Clean. Prod., 212, 1468-1480, 2019.

Liu, D. C., and Nocedal, J.: On the limited memory BFGS method for large scale optimisation, Math. Program., 45, 503–528, https://doi.org/10.1007/BF01589116, 1989.

Medlyn, B. E., Duursma, R. A., Eamus, D., Ellsworth, D. S., Prentice, I. C., Barton, C. V. M., Crous, K. Y., de Angelis, P., Freeman, M., and Wingate, L.: Reconciling the optimal and empirical approaches to modelling stomatal conductance, Glob. Change Biol., 17, 2134–2144, https://doi.org/10.1111/j.1365-2486.2010.02375.x, 2011.

Nuvolone, D., Petri, D., and Voller, F.: The effects of ozone on human health, Environ. Sci. Pollut. Res., 25, 175-196, https:/doi.org/10.1007/s11356-017-9239-3, 2018.

Oliver, R. J., Mercado, L. M., Clark, D. B., Huntingford, C., Taylor, C. M., Vidale, P. L., McGuire, P. C., Todt, M., Folwell, S., Shamsudheen Semeena, V., and Medlyn, B. E.: Improved representation of plant physiology in the JULES-vn5.6 land surface model: photosynthesis, stomatal conductance and thermal acclimation, Geosci. Model Dev., 15, 5567–5592, https://doi.org/10.5194/gmd-15-5567-2022, 2022.

Oliver, R. J., Mercado, L. M., Sitch, S., Simpson, D., Medlyn, B. E., Lin, Y.-S., and Folberth, G. A.**:** Large but decreasing effect of ozone on the European carbon sink, Biogeosciences, 15**,** 4245–4269, https://doi.org/10.5194/bg-15-4245-2018, 2018.

Op de Beeck, M., Gielen, B., Jonckheere, I., Samson, R., Janssens, I. A., and Ceulemans, R.: Needle age-related and seasonal photosynthetic capacity variation is negligible for modelling yearly gas exchange of a sparse temperate Scots pine forest, Biogeosciences, 7, 199–215, https://doi.org/10.5194/bg-7-199-2010, 2010.

Proietti, C., Anav, A., and De Marco, A.: The contribution of stomatal and non-stomatal pathways to ozone flux in different European forests, Sci. Total Environ., 799, 149326, 2021.

Proietti, C., Anav, A., Anav, A., Marco, A., Sicard, P., & Vitale, M.: A multi-sites analysis on the ozone effects on Gross Primary Production of European forests, The Science of the total environment, 556, 1-11 . https://doi.org/10.1016/j.scitotenv.2016.02.187, 2016.

Rannik, Ü., Altimir, N., Mammarella, I., Bäck, J., Rinne, J., Ruuskanen, T., Hari, P., Vesala, T., & Kulmala, M.: Ozone deposition into a boreal forest over a decade of observations: evaluating deposition partitioning and driving variables. *Atmospheric Chemistry and Physics*, 12, 12165-12182. https://doi.org/10.5194/ACP-12-12165-2012, 2012.

Savi, F., Nemitz, E., Coyle, M., Aitkenhead, M., Frumau, K., Gerosa, G., Finco, A., Gruening, C., Goded, I., Loubet, B., Stella, P., Ruuskanen, T., Weidinger, T., Horvath, L., Zenone, T., and Fares, S.: Neural network analysis to evaluate ozone damage to vegetation under different climatic conditions, Front. For. Glob. Change, 3, 42, https://doi.org/10.3389/ffgc.2020.00042, 2020.

Schraik, D., Wang, D., Hovi, A., and Rautiainen, M.: Quantifying stand-level clumping of boreal, hemiboreal and temperate European forest stands using terrestrial laser scanning, Agric. For. Meteorol., 339, 109564, doi:10.1016/j.agrformet.2023.109564, 2023.

Sellar, A. A., Jones, C. G., Mulcahy, J. P., Tang, Y., Yool, A., Wiltshire, A., O'Connor, F. M., Stringer, M., Hill, R., Palmieri, J., Woodward, S., de Mora, L., Kuhlbrodt, T., Rumbold, S. T., Kelley, D. I., Ellis, R., Johnson, C. E., Walton, J., Abraham, N. L., Andrews, M. B., Andrews, T., Archibald, A. T., Berthou, S., Burke, E., Blockley, E., Carslaw, K., Dalvi, M., Edwards, J., Folberth, G. A., Gedney, N., Griffiths, P. T., Harper, A. B., Hendry, M. A., Hewitt, A. J., Johnson, B., Jones, A., Jones, C. D., Keeble, J., Liddicoat, S., Morgenstern, O., Parker, R. J., Predoi, V., Robertson, E., Siahaan, A., Smith, R. S., Swaminathan, R., Woodhouse, M. T., Zeng, G., and Zerroukat, M.: UKESM1: Description and Evaluation of the U.K. Earth System Model, J. Adv. Model. Earth Sy., 11, 4513–4558, https://doi.org/10.1029/2019MS001739, 2019.

Shang, B., Agathokleous, E., Calatayud, V., Peng, J., Xu, Y., Li, S., Liu, S., & Feng, Z.: Drought mitigates the adverse effects of O3 on plant photosynthesis rather than growth: A global meta-analysis considering plant functional types, Plant, cell & environment, https://doi.org/10.1111/pce.14808, 2024.

Sicard, P., De Marco, A., Dalstein-Richier, L., Tagliaferro, F., Renou, C., & Paoletti, E.: An epidemiological assessment of stomatal ozone flux-based critical levels for visible ozone injury in Southern European forests, The Science of the total environment, 541, 729-741 . https://doi.org/10.1016/j.scitotenv.2015.09.113, 2016.

Sitch, S., Cox, P. M., Collins, W. J., and Huntingford, C.: Indirect radiative forcing of climate change through ozone effects on the land-carbon sink, Nature, 448, 791-794, https://doi.org/10.1038/nature06059, 2007.

Soudani, K., Delpierre, N., Berveiller, D., Hmimina, G., Pontailler, J.-Y., Seureau, L., Vincent, G., and Dufrêne, É.: A survey of proximal methods for monitoring leaf phenology in temperate deciduous forests, Biogeosciences, 18, 3391–3408, https://doi.org/10.5194/bg-18-3391-2021, 2021.

Verryckt, L., Beeck, M., Neirynck, J., Gielen, B., Roland, M., & Janssens, I.:. No impact of tropospheric ozone on the gross primary productivity of a Belgian pine forest. Biogeosciences, 14, 1839-1855, https://doi.org/10.5194/BG-14-1839-2017, 2017.

Vallat, R.. Pingouin: statistics in Python. Journal of Open Source Software, 3(31), 1026, https://doi.org/10.21105/joss.01026, 2018.

Van Dingenen, R., Dentener, F. J., Raes, F., Krol, M. C., Emberson, L., and Muller, J. F.: The global impact of ozone on agricultural crop yields under current and future air quality legislation, Atmos. Environ., 43, 604-618, https://doi.org/10.1016/j.atmosenv.2008.10.033, 2009.

https://doi.org/10.5194/egusphere-2025-1375
Preprint. Discussion started: 2 April 2025

Vargas, R., Sonnentag, O., Abramowitz, G., Carrara, A., Chen, J., Ciais, P., Correia, A., Keenan, T., Kobayashi, H., Ourcival, J., Papale, D., Pearson, D., Pereira, J., Piao, S., Rambal, S., & Baldocchi, D.: Drought Influences the Accuracy of Simulated Ecosystem Fluxes: A Model-Data Meta-analysis for Mediterranean Oak Woodlands. Ecosystems, 16, 749-764. https://doi.org/10.1007/s10021-013-9648-1, 2013.

Warm Winter 2020 Team, ICOS Ecosystem Thematic Centre.: Warm Winter 2020 ecosystem eddy covariance flux product for 73 stations in FLUXNET-Archive format—release 2022-1 (Version 1.0). ICOS Carbon Portal. https://doi.org/10.18160/2G60-ZHAK, 2022.

Wittig, V., Ainsworth, E., Naidu, S., Karnosky, D., & Long, S.: Quantifying the impact of current and future tropospheric ozone on tree biomass, growth, physiology and biochemistry: a quantitative meta-analysis. *Global Change Biology*, 15. https://doi.org/10.1111/j.1365-2486.2008.01774.x, 2009.

Wong, T. J., Roy, A., and Lefer, B. L.: Estimating biogenic VOC emissions from leaf, branch, and canopy scale measurements in an urban park, Atmos. Environ., 254, 118347, 2022.

Yue, X. and Unger, N.: Ozone vegetation damage effects on gross primary productivity in the United States, Atmos. Chem. Phys., 14, 9137–9153, https://doi.org/10.5194/acp-14-9137-2014, 2014.

Zhang, L., Brook, J. R., and Vet, R.: A revised parameterization for gaseous dry deposition in air-quality models, Atmos. Chem. Phys., 3, 2067–2082, https://doi.org/10.5194/acp-3-2067-2003, 2003.

Zhu, L., Zhao, W., Ma, X., and Li, H.: Effects of ozone pollution on crop yields and economic losses in China, Environ. Pollut., 305, 119267, 2022.